# Self-Interference Assessment and Mitigation in 3GPP IAB Deployments

Yekaterina Sadovaya†, Dmitri Moltchanov†, Hosein Nikopour⋆, Shu-ping Yeh⋆,
Wei Mao⋆, Oner Orhan⋆, Shilpa Talwar⋆, and Sergey Andreev†
†Tampere University, Tampere, Finland.
⋆Intel Corporation, Santa Clara, CA, USA.

***Abstract*—The high propagation losses and sensitivity to link blockage naturally require dense deployments of millimeter-wave (mmWave) 5G New Radio (NR) systems. One of the inherent challenges in these deployments is cost-efficient backhauling. Addressing this issue, 3GPP has recently proposed the concept of integrated access and backhaul (IAB) to reduce the deployment costs by enabling wireless backhaul. The efficient utilization of spectrum in these systems is conditional on the ability of IAB nodes to simultaneously receive signals on their sectoral antennas. In this paper, we investigate the interference caused by this functionality and identify countermeasures including angular and spatial diversities. Our numerical results demonstrate that the angular distance of $25^\circ$ between the user equipment (UE) served by adjacent sectoral antennas is sufficient to efficiently mitigate interference. A comparable reduction in the interference level can also be achieved by utilizing spatial diversity with antenna separation of at least $20$ m. By combining these methods, one can identify the target levels of angular and spatial diversities suitable for the particular deployment restrictions.**

***Index Terms*—New Radio, IAB, self-interference, spatial diversity, angular diversity**

## I. Introduction

The fifth-generation (5G) New Radio (NR) systems are expected to deliver a decisive capacity boost at the air interface by utilizing the resource-rich millimeter-wave (mmWave) spectrum [1]. These frequencies, however, are characterized by much higher free-space, reflection, and penetration losses, as well as blockage-induced degradation, [2], thus severely limiting the coverage of prospective 5G NR base stations. As the standardization efforts are expected to conclude soon [3], the matter of cost-efficient deployment of such systems in practical environments becomes essential.

Extremely complex propagation conditions make direct network densification based on the small-cell concept expensive for the network operators [4]. Another approach to ensure the coverage extension of mmWave NR systems is to employ the integrated access and backhaul (IAB) technology recently ratified by 3GPP [5]. In this concept, the new entities (IAB nodes) serve as relays between remote UEs and the donor gNB (DgNB). In order to keep the capital expenditures reasonable, IAB nodes utilize wireless backhaul links, which are integrated with the radio access network (RAN).

Preliminary studies addressing 3GPP IAB performance [6]–[8] demonstrate that this approach allows to not only drastically extend the coverage of mmWave NR deployments but also significantly improve the UE data rates. However, as a result of the bottleneck at wireless backhaul connections, this parameter saturates much faster with the increased density of DgNBs [9] as compared to a fiber-backhaul approach. Therefore, efficient resource allocation between access and backhaul is becoming a crucial aspect for the efficient utilization of prospective 3GPP IAB architectures.

One of the ways to improve the performance of mmWave 3GPP IAB system is to re-utilize the available resources at both access and backhaul interfaces. This functionality requires the ability of IAB nodes to simultaneously receive signals from access and backhaul links on all its sectoral antennas. Hence, in addition to the interference from other cells [10], [11], self-interference (SI) may hamper efficient resource utilization in 3GPP IAB architectures. In [12], dynamically reconfigured beam steering antennas have been proposed for SI suppression. The authors of [13] derived the probability density function of SINR by taking into account SI. However, in these studies, the authors did not consider the inherent technological specifics of the 3GPP IAB operation.

The aim of this study is to comprehensively characterize SI in 3GPP IAB systems. To this aim, we develop and calibrate a system-level simulation (SLS) tool that captures deployment and propagation features of the reference 3GPP deployment scenario. We then proceed to evaluate the impact of angular and spatial diversities at IAB nodes.

The main contributions of this work are the following:

- We characterize interference caused by simultaneous reception from the neighboring antenna sectors of the IAB node and investigate two interference mitigation techniques – spatial and angular diversities.
- We demonstrate that $25^\circ$ of angular separation and $20$ m of spatial antenna separation lead to effective interference mitigation performance. By combining these methods, one can identify the target level of angular and spatial diversities suitable for given deployment restrictions.

The rest of this paper is organized as follows. Section II overviews the reference 3GPP IAB architecture. Then, in Section III, we describe the deployment utilized in our study. The SLS implementation of the 3GPP IAB technology is introduced in Section IV. We report and discuss the numerical results in Section V. Conclusions are drawn in the last section.

## II. 3GPP IAB Architecture

3GPP IAB architecture introduces an additional entity in the cellular system named IAB node [5]. The specification of IAB nodes assumes the reuse of existing functions and interfaces, which were initially defined for the access interface. These functionalities include mobile-termination (MT), user plane function (UPF), session management function (SMF), and access and mobility management function (AMF). The basic interfaces involved are NR Uu, F1, NG, X2, and N4. In the context of IAB, the MT function implies the termination of the backhaul Uu radio interface layers directed to the IAB-donor or other IAB nodes. The SMF is responsible for protocol data unit (PDU) sessions. The user plane (UP) data and quality of service (QoS) are handled by the UPF. The AMF is responsible for control plane (CP) functions, i.e., mobility management, security, and authentication control.

An example of IAB architecture in stand-alone (SA) mode with the required interfaces is given in Fig. 1. In non-SA mode, the IAB node utilizes the NR link only for the backhaul links. The IAB-donor can be a single logical node, i.e., a central unit (CU), or it may comprise of a CU and several distributed units (DUs). A CU is connected to the core network (CN) via the NG interface and is responsible for radio resource control (RRC), packet data convergence protocol (PDCP), and service data adaptation protocol (SDAP). The motivation for splitting DU and CU functionalities lies in the fact that time-critical operations such as scheduling can be implemented in the DU while less crucial functions are separated in the CU.

Since the overall system performance depends on the number of hops between the IAB node and the DgNB, topology establishment and multi-hop operation are essential aspects of IAB systems. Each IAB node bears two functions: MT and DU. The MT part is responsible for the communication with a parent while the DU part is intended for the communication with a child IAB node or UE. An IAB node multiplexes UE data radio bearers (DRBs) to the backhaul RLC channels. The backhaul RLC channels are employed for the transportation of packets between IAB nodes and DgNB.

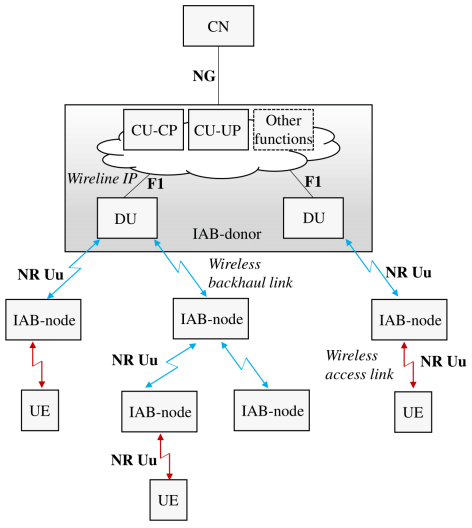


Fig. 1: Reference IAB architectures in SA mode [5].

To establish an IAB network, the following steps should be completed. First, the MT of an IAB node determines a parent node. Then, an RRC connection with the CU is requested through the selected parent. In its turn, the backhaul link is established using the RLC. This is followed by a new routing protocol, which is known as the backhaul adaptation protocol (BAP). BAP is responsible for the packet forwarding over multiple hops between the DgNB and the IAB node. At the next stage, the DU function at the IAB node is set up. The latter procedure implies the establishment of the F1-C connection. Once the topology is configured, it can be further adapted based on the environmental conditions and the load. In order to accomplish that, information about the link quality and the load of the IAB node is transmitted by the MT of an IAB node to the CU. This enables the CU to allocate resources efficiently.

In order to support operations at the same frequency, the access and the backhaul traffic should be multiplexed. On the other hand, to ensure the feasibility of the handover procedure, an IAB node should operate under a half-duplex (HD) constraint. The solution for resource partitioning recommended by the 3GPP is time-division multiple access (TDMA) [5]. However, the IAB node can simultaneously transmit or receive traffic from each of its antenna sectors. Therefore, the following transmissions are possible in the first part of the frame: from DgNB to UE; from DgNB to IAB node; and from UE to IAB node. The second part corresponds to the opposite transmissions, respectively. Additionally, multi-beam scenarios inherent to 5G NR are feasible for IAB deployments. However, excess beams at the IAB node can reduce the transmit power as it is being split between a number of beams.

## III. System Model

In this section, our modeling approach is described step-by-step. First, we outline the scenario and implementation details. Then, radio propagation-related aspects are discussed, such as propagation model, antenna configuration, and UE mobility.

*1) 3GPP IAB Deployment:* Our deployment of interest is depicted in Fig. 2. We consider a single IAB node as our aim is to characterize SI and the methods to mitigate it. Therefore, it is sufficient to consider an IAB node in isolation. The IAB node is placed in the center. The DgNB and the IAB node are separated from each other by the distance of $R$. The DgNB is placed at the edge of the cell and points at the cell by one of its antenna sectors. $R$ is chosen such that no UEs experience an outage within this radius. The antenna employed at an IAB node is sectorized. UEs served by the same sector are multiplexed via TDMA. The UEs are assumed to be mobile. We also account for the HD constraint, i.e., an IAB node can either receive or transmit at a time.

*2) Propagation Model:* In our system, the channel is modeled according to the 3GPP cluster channel model [14]. The large-scale parameters (LSPs) and small-scale parameters (SSPs) correspond to the UMa LoS setup. Hence, the path

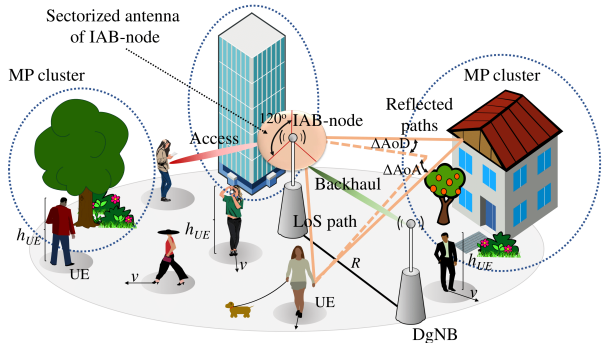


Fig. 2: Considered 3GPP IAB deployment.

loss (PL) for each DgNB-UE or IAB-UE link is calculated as follows

$$L_{UMa-LoS} = \begin{cases} L_1, & 10 \text{ m} \leq d_{2D} \leq d_{BP} \\ L_2, & d_{BP} \leq d_{2D} \leq 5 \text{ km}, \end{cases} \quad (1)$$

where the branches are given by

$$\begin{aligned} L_1 &= 28 + 22\log_{10}(d_{3D}) + 20log_{10}(f_c), \\ L_2 &= 28 + 40\log_{10}(d_{3D}) + 20\log_{10}(f_c) - \\ &- 9(\log_{10}(d_{BP})^2 - (h_{BS} - h_{UE})^2), \end{aligned} \quad (2)$$

while $d_{2D}$ and $d_{3D}$ are the corresponding 2D and 3D distances from UE to IAB node or DgNB, $f_c$ is the carrier frequency in MHz, and the breakpoint distance $d_{BP}$ is given as

$$d_{BP} = 4\frac{h_{BS}h_{UE}f_c}{c}, \quad (3)$$

where $h_{BS}$ is the height of either $h_{DgNB}$ or $h_{IAB}$ in m; $c$ is the speed of light.

Then, the correlated LSPs required for multipath (MP) cluster formation are generated. These LSPs include the delay spread (DS), AoA and AoD spreads in azimuth and zenith planes, shadow fading (SF), and Ricean K-factor [14]. The relation between the LSPs is further described with the correlation coefficient matrix, which is calculated using the Cholesky decomposition. The LSPs for different IAB-UE and DgNB-UE links are uncorrelated.

In order to obtain MP components (MPCs), SSPs should be generated. The delays of each cluster $n$ are chosen randomly from the delay distribution defined in [14]. Hence, the $n$-th cluster delay reads as

$$\tau_n = -r_\tau \text{DS} \ln(X_n), \quad (4)$$

where $r_t$ is the delay distribution proportionality factor and $X_n \sim U(0,1)$. The corresponding power of the $n$-th cluster is

$$P_n = \exp\left(-\tau\frac{r_\tau - 1}{r_\tau \text{DS}}\right) 10^{-\frac{Z_n}{10}}, \quad (5)$$

where $Z_n$ is the shadow fading per cluster in dB.

Similarly, the power angular spectrum is generated as a wrapped Gaussian variable. For example, AoAs are defined using the inverse Gaussian function as

$$\phi_{AoA_n} = 2(\text{ASA}/1.4)\sqrt{-\ln(P_n/\max(P_n))}, \quad (6)$$

where ASA stands for AoA spread in the azimuth plane. The rays are further coupled together randomly within a cluster. Then, each MPC in a cluster is initialized with a cross-polarization power ratio (XPR). Finally, channel coefficients are obtained from the LSPs and SSPs. It is worth noting that UE mobility is also included into our model. Therefore, spatial and temporal consistency should be preserved. For this purpose, we use the consistency procedure A from [14].

*3) Antenna Model:* An antenna array in our setup is modeled according to [14]. Therefore, the array factor is

$$\tilde{W} = VW, \quad (7)$$

where $V(\phi,\theta) = [v_{1,1}, v_{1,2}, ...., v_{N_H,N_V}]^T$ is the phase shift due to array placement and $W = [w_{1,1}, w_{1,2}, ...., w_{N_H,N_V}]^T$ is the weighting factor; $N_H, N_V$ are the total numbers of antenna elements; $\phi, \theta$ are the angular shifts in horizontal and vertical planes, correspondingly.

The phase shift is defined as

$$\begin{aligned} v_{m,n} = \exp\Big[ -2i\pi\Big((n-1)\frac{d_V}{\lambda}\cos(\theta) + \\ + (m-1)\frac{d_H}{\lambda}\sin(\theta)\sin(\phi)\Big)\Big], \end{aligned} \quad (8)$$

where $m = 1, 2, ...N_H$, $n = 1, 2, ...N_V$. The weight $w_{m,n}$ can be determined with the following equation:

$$\begin{aligned} w_{m,n} = \frac{1}{\sqrt{N_H N_V}}\exp\Big[2i\pi\Big((n-1)\frac{d_V}{\lambda}\cos(\theta_{tilt}) + \\ + (m-1)\frac{d_H}{\lambda}\sin(\theta_{tilt})\sin(\phi_{scan})\Big)\Big], \end{aligned} \quad (9)$$

where $\phi_{scan}$ and $\theta_{tilt}$ are the horizontal and vertical steering.

Denoting the transmitted signal at each antenna by $S(t) = [S_{1,1}, S_{1,2}, ...., S_{N_H,N_V}]^T$, the output of the antenna array is

$$\begin{aligned} y(\phi,\theta,t) = \sum_{m=1}^{N_H}\sum_{n=1}^{N_V} S_{m,n}(t)w_{m,n}E_{m,n}(\phi,\theta) = \\ - P_E(\phi,\theta)\tilde{W}^H S(t), \end{aligned} \quad (10)$$

where $E_{m,n}$ is the complex gain of the element pattern. In turn, the value of $E_{m,n}$ is directly affected by the configuration of the element pattern, which is set by 3GPP [14] as

$$A_E(\phi,\theta) = G_E - min[-(A_{E_H}(\phi) + A_{E_V}), A_{max}], \quad (11)$$

where $G_E$ = 8 dBi is the maximum directional gain of the element pattern; $A_{E_H}$ and $A_{E_V}$ are the attenuations in horizontal and vertical directions; $A_m$ = 30 dB is the front to back ratio. With the utilized configuration, the half-power beamwidth (HPBW) of the resultant array is affected by the number of antenna elements. The antenna arrays employed at the UE, DgNB, and IAB nodes are given in Table I.

*4) UE Mobility Model:* As mentioned above, the UEs are mobile in our deployment. Specifically, it is assumed that the mobility pattern follows the random direction mobility (RDM) model [15]. The RDM is an extension of the Pearson-Rayleigh random walk model, which is able to capture the temporal behavior of UEs. Accordingly, the UE first chooses

the movement direction, which is selected randomly via the uniform distribution between 0 and $2\pi$. Then, the UE moves in this direction for an exponentially distributed amount of time $\tau$ with the speed of $\nu$. The speed is chosen randomly via the Gaussian distribution with $\mu$ and $\sigma$ in every time interval $\tau$. We set the average speed of UEs to 3 km/h in our modeling. When the UE reaches the edge of the considered area, its direction of movement is reversed.

## IV. SLS Implementation

Our developed framework is based on the discrete-event simulation (DES) technique. The software is developed by using Python programming language with multi-thread optimizations. A simulation campaign has also been carried out to obtain the metrics of interest by relying on the following procedure. First, we specify the input parameters, such as positions of the IAB node and the IAB donor, antenna gains, width of the antenna sector, etc. The full list of parameters is given in Table I. Once the system is initialized, associations are established at the time instant $t = 0$ based on the maximum RSRP criterion. Tx and Rx antennas are assumed to be aligned in the transmission direction. Then, the simulation is launched under the consideration of UE mobility. This factor degrades the signal quality as the distance to UE continually evolves in time; thus, the RSRP for each UE is updated every transmission time interval (TTI). We assume that UEs are assigned to their initial association points and no handover occurs during a simulation run. The single run simulation time is set to $t = 1800$ s. The method of replications is utilized to determine time-averaged statistics with the number of replications set to 50.

In our simulations, the HD operation mode is assumed. Hence, each time slot is divided into two parts with the division coefficient of 0.5 for DL and UL. In the first part of the slot, the DgNB transmits to the UEs and the IAB node while the IAB node receives from the DgNB and its child UEs. In the second part, the IAB node transmits to its served UEs and the DgNB. Time resources are divided equally between the active UEs. The IAB node antenna consists of 3 sectors, where each antenna sector has its own directional pattern, i.e., antenna beam. The latter assumption implies three beams at the IAB node, which enables simultaneous reception by each antenna sector of the IAB node.

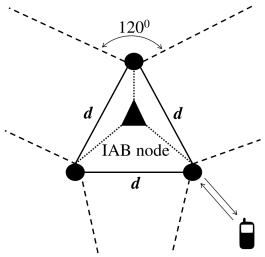


(a) Spatial diversity.

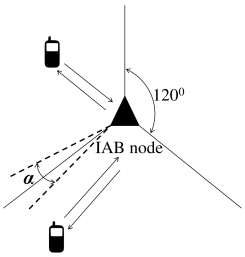


(b) Scheduling diversity.

Fig. 3: Illustration of spatial (a) and angular (b) diversities.

TABLE I: Parameters utilized in numerical assessment.

| Parameter | Value |
|---|---|
| Carrier frequency, $f_c$ | 30 GHz |
| Bandwidth, $B$ | 400 MHz |
| Number of UEs | 30 |
| Cell radius, $R$ | 500 m |
| Tx power of DgNB, $P_D$ | 40 dBm |
| Tx power of IAB, $P_{IAB}$ | 33 dBm |
| Tx power of UE, $P_{UE}$ | 23 dBm |
| Noise figure of DgNB and IAB, $NF_{BS}$ | 7 dB |
| Noise figure of UE, $NF_{UE}$ | 13 dB |
| Power spectral density of noise, $N_0$ | -173.93 dBm/Hz |
| Antenna array of UE | 4x4 |
| Antenna array of DgNB and IAB | 16x16 |
| Velocity of UE, $v$ | 0.83 m/s |
| Height of DgNB, $h_{DgNB}$ | 25 m |
| Height of IAB, $h_{IAB}$ | 10 m |
| Height of UE, $h_{UE}$ | 1.5 m |

In addition, two approaches to decreasing inter-sector interference are considered, namely, spatial and angular diversities. The first method presumes physical antenna separation at the IAB node. To enable it, we consider that antenna arrays form an equilateral triangle with the IAB node equipment placed in the center of the mass. This is assumed to minimize the cable losses. The angular separation refers to specifying the minimum angular distance between the UEs associated with the adjacent antenna arrays scheduled for transmission. By ensuring a certain angular distance, we imply that only those UEs which have greater angular distance can be serviced simultaneously at the adjacent arrays. The described diversity techniques are illustrated in Fig. 3.

To assess the overall system performance, we first proceed by characterizing the cumulative distribution function (CDF) of SINR and its tail with and without interference mitigation techniques. Then, in a more detailed assessment of the interference mitigation schemes, we concentrate on time-series representation of interference by comparing the behavior of SNR and SINR values, where the latter explicitly accounts for interference coming from all the sources including simultaneous reception at the adjacent sectors. The system parameters are thus the angular distance between the scheduled UE at the

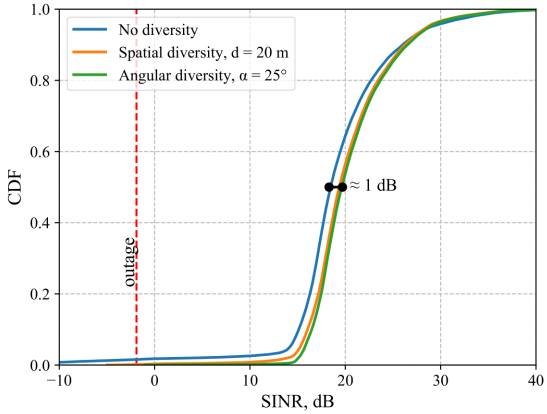


Fig. 4: CDF of SINR averaged over time.

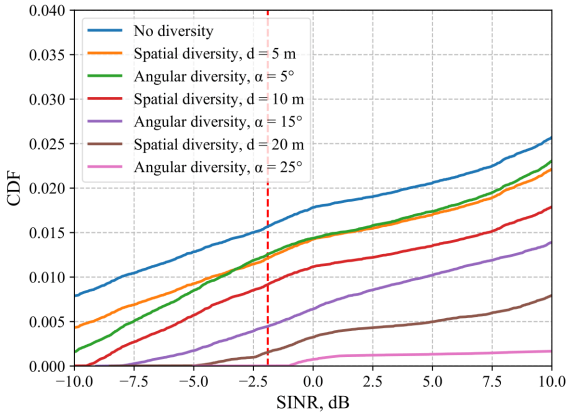


Fig. 5: CDF of SINR scaled from -10 dB to 10 dB.

same IAB node and the planar distance between the antenna elements at the IAB nodes.

## V. Numerical Results

In this section, we report the numerical results for SI at the IAB nodes. The system parameters are provided in Table I.

### A. Time-Averaged Results

The CDFs of SINR for SI with and without interference reduction schemes are shown in Fig. 4, where the antenna array spatial separation is set to $d = 20$ m, while the angular distance between UEs is $\alpha = 25°$. As one may observe, the difference between the SINR curves corresponding to the considered interference mitigation schemes is just around 1 dB for both approaches. While the average behavior is not affected significantly, the UEs may experience an outage situation regularly. This can be seen in Fig. 5, which shows the tail of the SINR distribution. The outage boundary is defined according to the modulation and coding scheme (MCS) table [16] and corresponds to the lower threshold of the smallest channel quality indicator (CQI) index. As can be seen in Fig. 5, smaller diversity also reduces SI. However, with spatial diversity of $d = 5$ m or angular diversity of $\alpha = 5°$, the SI is only 1.2 times as lower compared to the situation where

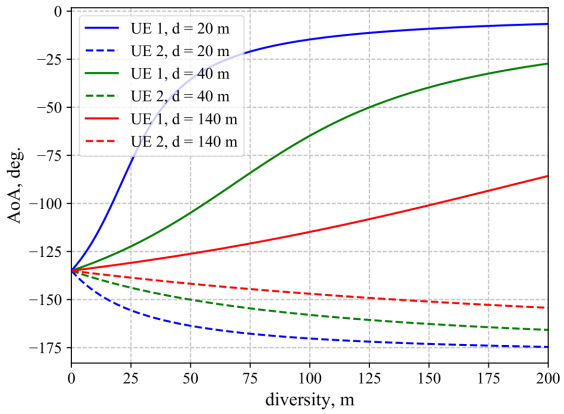


Fig. 6: AoA as a function of spatial diversity.

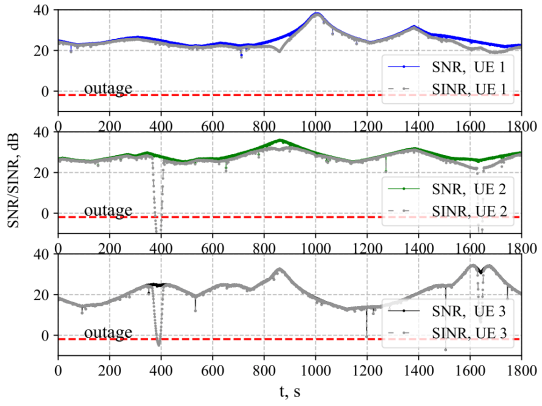


(a) SINR and SNR without antenna diversity.

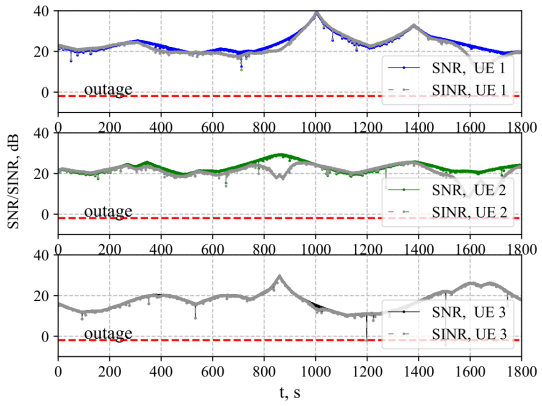


(b) SINR and SNR with 20 m antenna diversity.

Fig. 7: SINR as a function of angular distance for 3 different UEs.

no diversity is applied. In order to reduce SI by 10 times, the values of $d = 20$ m and $\alpha = 25°$ are recommended.

We now proceed with studying this effect in detail and identifying the desired angular and antenna separations by using the SINR time series. We would like to illustrate that for static UE locations the angular distance between UEs heavily depends on the spatial redundancy. This effect is shown in Fig. 6 where the former metric is displayed as a function of the distance between antennas at the IAB node for three distances from UEs to IAB nodes, 20, 50, and 140 m. As one may observe, in general, these two parameters induce a trade-off for system designers. Particularly, the higher the separation distance between sectoral antennas is, the smaller angular distance for simultaneously scheduled UEs can be used. The latter may relax requirements for UE scheduling at IAB nodes.

### B. Time-Dependent Behavior

The time-dependent behavior of AoA and SINR for the UEs associated with the adjacent antenna sectors of an IAB node is depicted in Fig. 8a. As one may notice, the SINR curve follows closely that of the SNR most of the time. The only exception is when the angular distance between the UEs starts to decrease. In these cases, one may observe occasional spikes in the SINR behavior. This implies that the interference increases

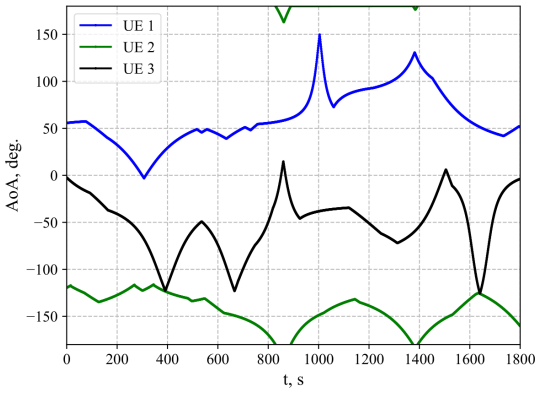


(a) AoA without antenna diversity.

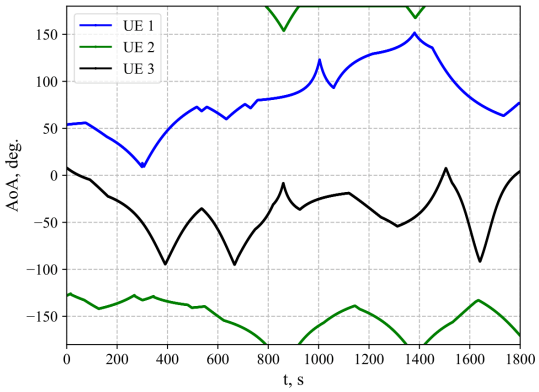


(b) AoA with 20 m antenna diversity.

Fig. 8: AoA as a function of angular distance for 3 different UEs.

greatly. The identified threshold in the angular distance when simultaneous reception begins to affect the performance of the system is $25^\circ$, see Fig. 5.

The time-dependent behavior of AoA and SINR for the UEs associated with the adjacent antenna sectors of an IAB node for the antenna separation distance of 20 m is illustrated in Fig. 8b and Fig. 7b. As one may observe, already for a relatively small separation distance of 20 m, the angular threshold after which the interference starts to play a major role reduces drastically. For example, SINR at $t = 400$ s in Fig. 7b is increased by 20 dB. However, note that this value may heavily depend on the current UE-BS distances as shown in Fig. 6.

Summarizing, one may observe that the level of interference becomes notable when the inter-UE angular distance shrinks under $25^\circ$ when no planar antenna separation is utilized at the IAB nodes. Furthermore, by adding a 20 m separation distance between the antennas, the angular distance between the UEs is kept larger. To fully utilize all the system bandwidth at all sectoral antennas, one has to make sure that no UEs located closer than the critical distance are scheduled for transmission simultaneously.

## ACKNOWLEDGEMENT

This work was supported by Intel Corporation and the Academy of Finland (project IDEA-MILL).

## VI. CONCLUSION

One of the crucial design considerations allowing to increase the capacity of 3GPP IAB networks is the utilization of simultaneous signal reception of the IAB nodes. This potentially enables the leverage of the full bandwidth available in the system at all times serving both backhaul and access simultaneously. In this paper, we assessed the effect of simultaneous transmission in adjacent sectors of the IAB nodes on the SINR. The key findings can be summarized as follows. The average impact from the simultaneous reception on the SINR is relatively small, i.e., around 1 dB. However, certain UEs may still frequently experience outage conditions. To alleviate these, one could utilize either spatial or angular diversity. Particularly, the angular distance of $25^\circ$ is sufficient to mitigate SI. A comparable reduction in SI can be achieved by utilizing the antenna separation of at least 20 m. By employing these methods, one can identify the target levels of angular and spatial diversities suitable for given deployment restrictions.

## REFERENCES

[1] S. Rangan, T. S. Rappaport, and E. Erkip, "Millimeter-wave cellular wireless networks: Potentials and challenges," *Proceedings of the IEEE*, vol. 102, no. 3, pp. 366–385, 2014.

[2] M. Gapeyenko, A. Samuylov, M. Gerasimenko, D. Moltchanov, S. Singh, E. Aryafar, S.-p. Yeh, N. Himayat, S. Andreev, and Y. Koucheryavy, "Analysis of human-body blockage in urban millimeter-wave cellular communications," in *2016 IEEE ICC*, pp. 1–7, IEEE, 2016.

[3] 3GPP, "Summary of Rel-16 work items (Release 16)," *3GPP TR 21.916 V0.5.0*, 2020.

[4] D. López-Pérez, M. Ding, H. Claussen, and A. H. Jafari, "Towards 1 Gbps/UE in cellular systems: Understanding ultra-dense small cell deployments," *IEEE Communications Surveys & Tutorials*, vol. 17, no. 4, pp. 2078–2101, 2015.

[5] 3GPP, "Study on integrated access and backhaul (Release 16)," *3GPP TR 38.874 V16.0.0*, 2018.

[6] M. Polese, M. Giordani, A. Roy, S. Goyal, D. Castor, and M. Zorzi, "End-to-end simulation of integrated access and backhaul at mmwaves," in *2018 IEEE CAMAD*, pp. 1–7, IEEE, 2018.

[7] M. Polese, M. Giordani, T. Zugno, A. Roy, S. Goyal, D. Castor, and M. Zorzi, "Integrated access and backhaul in 5G mmwave networks: Potential and challenges," *IEEE Communications Magazine*, vol. 58, no. 3, pp. 62–68, 2020.

[8] M. N. Islam, N. Abedini, G. Hampel, S. Subramanian, and J. Li, "Investigation of performance in integrated access and backhaul networks," in *2018 IEEE INFOCOM*, pp. 597–602, IEEE, 2018.

[9] C. Saha and H. S. Dhillon, "Millimeter wave integrated access and backhaul in 5G: Performance analysis and design insights," *IEEE JSAC*, vol. 37, no. 12, pp. 2669–2684, 2019.

[10] E. Kalantari, I. Bor-Yaliniz, A. Yongacoglu, and H. Yanikomeroglu, "User association and bandwidth allocation for terrestrial and aerial base stations with backhaul considerations," in *2017 IEEE 28th Annual International Symposium on PIMRC*, pp. 1–6, IEEE, 2017.

[11] A. Fouda, A. S. Ibrahim, İ. Güvenç, and M. Ghosh, "Interference management in UAV-assisted integrated access and backhaul cellular networks," *IEEE Access*, vol. 7, pp. 104553–104566, 2019.

[12] S. Shaboyan, A. S. Behbahani, and A. M. Eltawil, "Practical considerations for full duplex enabled 5G integrated access and backhaul," *Journal of Signal Processing Systems*, pp. 1–10, 2020.

[13] X. Zhang, F. Liu, and H. Xia, "Ergodic capacity analysis for full-duplex integrated access and backhaul system," in *2019 IEEE Global Conference on Signal and Information Processing*, pp. 1–5, 2019.

[14] 3GPP, "Study on channel model for frequencies from 0.5 to 100 GHz (Release 15)," *3GPP TR 138.901 V15.0.0*, 2018.

[15] R. R. Roy, *Handbook of mobile ad hoc networks for mobility models*, vol. 170. Springer, 2011.

[16] 3GPP, "Study on new radio access technology physical layer aspects (Release 14)," *3GPP TR 38.802 V14.2.0*, 2017.